Imaging of Polycarbonate Track Etch Membranes with Atomic Force Microscopy

Kaimeng Zhou

Advisor: S.C. Jacobson

C500 Final Report

April 22, 2004

Introduction

Atomic force microscopy (AFM) is a type of scanning probe microscopy in which a small tip is scanning across the sample to obtain information about the surface. The information gathered from the interaction between the tip and the surface can be simply physical topography. Furthermore, the sample's physical properties, chemical properties and magnetic properties can also be gathered from AFM, through different working modes. There are many other techniques employed for gathering surface information of a sample, such as Scanning electron microscopy (SEM) and Sum frequency generation (SFG). The advantage of AFM over other techniques is that AFM tip can be used to characterize a small area of interest. Stochastic sensing using PCTE membranes has recently been reviewed.[1] We are interested in a variant of these methods that combines coulter counting and chromatography, i.e., nanopore chromatography. With nanopore chromatography, the presence of single molecule or ion can be determined by applying a constant voltage across the pore and monitoring the current through the pore. Several groups have already done some sensing based on nanopore membranes, for instance, size exclusion separation of proteins using nanopore membrane[2] and charge-based separation.[3-4] People had also performed nanopore separation using molecular recognition, such as enzymatic molecular recognition,[5] chiral separation,[6-7] separation of nucleic acids.[8] However, people are still not clear about how these particles will interact with the nanopore, for example, how does the particle size determine the current amplitude and how do the chemical properties of the particle and membrane affect the transit time. In our experiment, all these mechanisms will be studied.
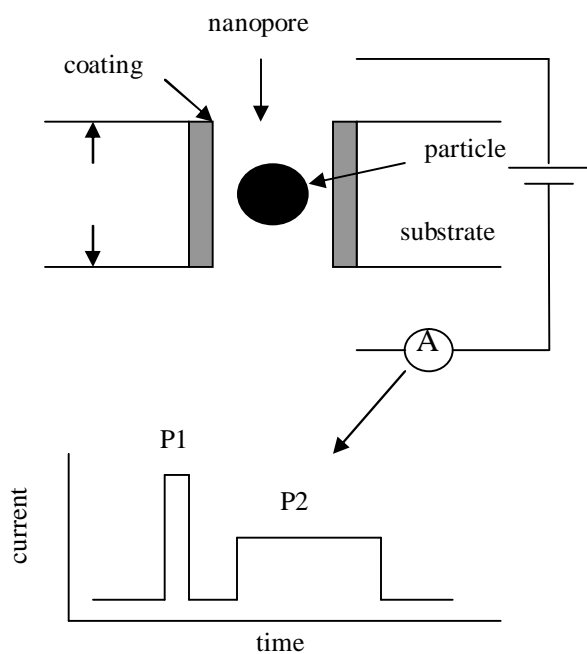
Figure 1. Schematic of a Nanopore device (top) and the variation of current with time for particle P1 and P2 (bottom)

The basic design of nanopore device is shown in Figure 1, polycarbonate membrane is used and glass slide is used as substrate. The wall of the nanopore can be coated with different substances to introduce chemical selectivity, e.g., hydrophobic, hydrophilic, or ionic. The size of the particle can be detected by the amplitude of the current across the pore. The larger the particle, the larger the amplitude. The interaction between the particle and the wall/coating can be determined by transit time. As shown in Figure 1, particle P1 does not interact with the wall/coating and has a shorter transit time when it passes through the pore, while particle P2 interacts with the wall/coating and has a longer transit time when it passes through the pore.

We are also interested in multilayer membrane separation. Multilayer membrane separation will significantly increase the selectivity of the device, which will enable us to identify or separate a more general type of species, as shown in Figure 2.

Figure 2. Schematic of multilayer membrane device
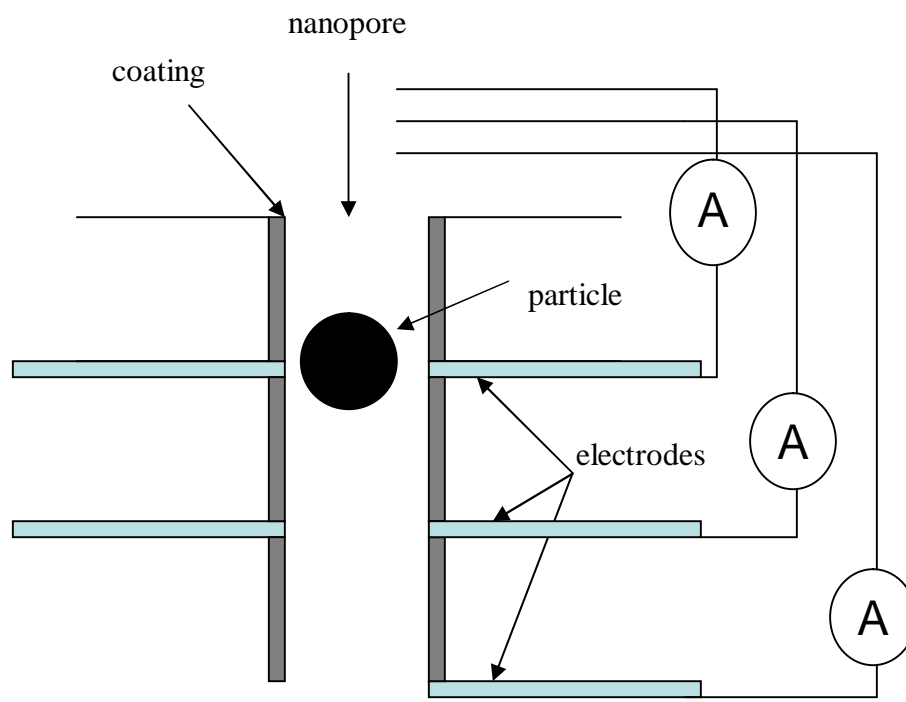
A voltage is applied across the multilayer pore with different coatings. The current through the each pore is monitored. In this case, information of each pore can be obtained by the current-time diagram. With this method we could possibly create fingerprint of any given component using this device if we have a better understanding of interactions between the wall/coating and the particles. In order to make this nanopore device, we should first be able to isolate a single nanopore or several adjacent nanopores. AFM can accomplish this task. Using AFM we can first image a small area with a single pore or several pores. Then we can apply a voltage at the AFM tip and monitor the current. In this report, we mainly focus on the imaging polycarbonate track etch (PCTE) membranes using AFM and discuss the factors that affect the image resolution. We studied sample preparation, scan size, scan rate, integral gain and set point and how these factors can be optimized.

Experimental

I. Materials. Microscope slides (12-549, Fisher Scientific), polycarbonate track etch (PCTE) membranes with 10, 50, 100 nm pores (Osmonics, Inc.), double-sided carbon tape, and packing tape (Scotch 3710 and 3750, 3M) were used in the experiments.

II. Instrumentation. AFM experiments were conducted and analyzed by MFP-3D™ Stand Alone Atomic Force Microscope (Asylum Research INC). Silicon tips with a 2 N/m spring constant, 70 kHz resonant frequency and 240 nm length (Olympus AC240TS), and with a 42 N/m spring constant, 300 kHz resonant frequency and 160 nm length (Olympus AC160TS), were used to acquire the images in tapping mode.

III. Sample Preparation

Several methods were used to hold the samples for AFM imaging.

1. Microscope glass slides (75 mm x 25 mm x 1 mm) were used as the substrate, and a PCTE membrane was placed on the slide. Packing tape (3710, 48 µm thick) was used to cover the membrane to firmly attach the membrane to the slide, as shown in figure 3. A small hole (about 100 µm in radius) was made in the tape by burning it with laser beam so that the AFM tip could press on the surface of the membrane.
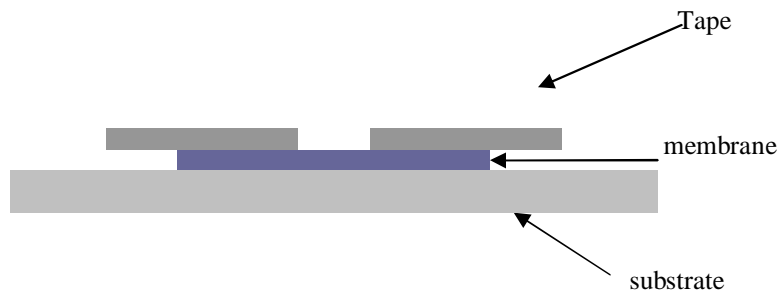
Figure 3. Schematic of sample preparation method 1, PCTE membrane was placed on the glass side substrate and packing tape 3710 with a small hole was placed above the membrane.

2. A second packing tape (3750, 72 µm thick) was used, and the same procedures as the first method were followed to prepare the sample.

3. As shown in figure 4, microscope glass slide was still used as the substrate but double-sided carbon tape was placed on the slide under the PCTE membrane. The PCTE membrane was then placed on the carbon two-side tape and was very well attached to the tape.
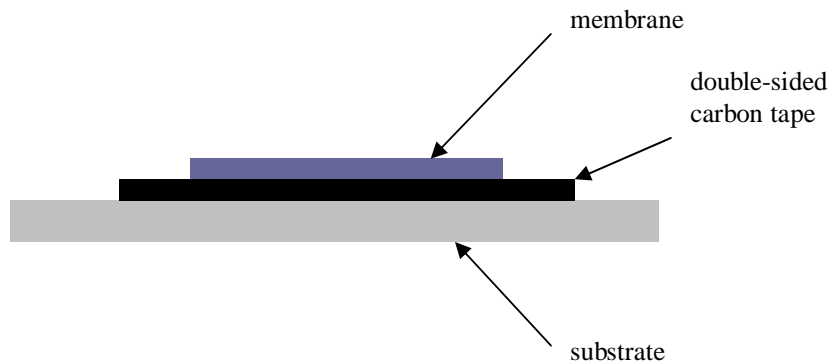

Figure 4. Schematic of sample preparation method 3, PCTE membrane was attached to the glass slide substrate with the help of double-sided carbon tape

IV. AFM methodology

1. AFM working principle[9-10]. AFM obtains information about the surface from the interaction between the surface and the tip. This kind of interaction is expressed by the motion of

814

the cantilever which is measured by a "light lever" method. In this method, a laser beam is directed to the backside of the cantilever near the tip and reflected onto a photon detector, as shown in Figure 5.

laser
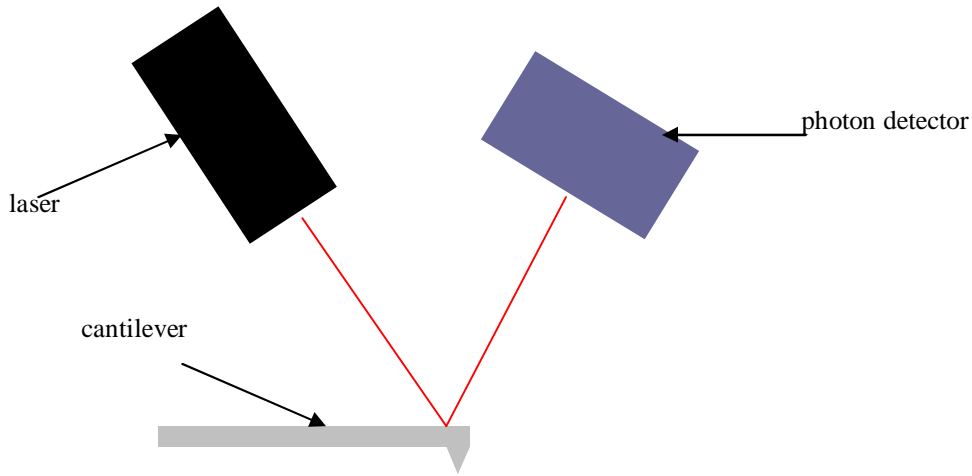
cantilever

photon detector

Figure 5. The light lever sensor uses a laser beam to monitor
the deflection of the cantilever

The laser beam will be reflected to different spots of the photon detector when the cantilever bends, thus the photon detector can monitor the motion of the cantilever.

2. AFM Working Modes. There are two important working modes of AFM, contact mode and tapping mode. Figure 6a shows how the AFM in contact mode works. During the scan, a constant force is applied to the surface. The tip directly follows the topography of the surface as it is scanning, resulting in cantilever deflection. In contact mode, the sample is scanned with a fixed cantilever deflection and also with a constant force applied to the surface during the scan. Surface information can be obtained by the feedback information because feedback of the system controls the cantilever deflection.

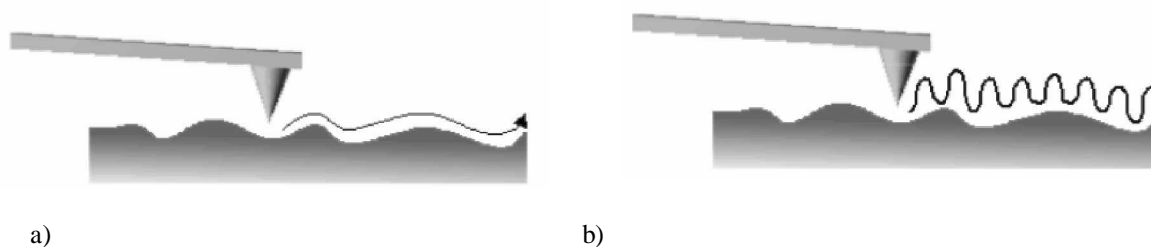a)   b)

Figure 6. Illustration of working modes of AFM. (a) represents the motion of tip in contact mode AFM and (b) represents the motion of tip in tapping mode AFM

815

Figure 6b shows how tapping mode AFM works. The cantilever keeps vibrating when the tip is scanning across the surface, the signal is measured at every point when the tip is down to the surface. When the vibrating cantilever comes close to the surface, the amplitude and phase of the vibrating cantilever may change. Those changes in the vibration amplitude or phase are recorded because the changes are related to the force applied to the surface.

AFM imaging in air was performed in tapping mode (intermittent contact or non-contact mode) with 7 nm tetra tip scanning over the membrane surface. Two types of tips were used to acquire images. One is 240 nm long silicon tip with a resonant frequency of 70 kHz, the other is 160 nm short silicon tip with a resonance frequency of 300 kHz. In order to prevent deep penetration into the membrane and breaking the tip, low driving amplitude was set to establish surface contact. The set point is set to 800 mV for all the scans at the beginning. After engaging the tip, Z-voltage was slowly tuned down to around 40-50 mV. The scan rate is set to 1.0 Hz at the beginning to verify the contact with the surface. During the scan, the scan rate was tuned to achieve the best resolution. For the images, 512 x 512 points or 256 x 256 points were taken. Integral gain is tuned during the scan. The initial value of integral gain was set to 10. For different scan size, all the above parameters should be well-tuned to improve the resolution.

Results

1. Images of sample 1 (tape#3710--membrane--glass slide). A PCTE membrane with 100 nm pores and a silicon 240 nm tetra tip with resonant frequency of 70 kHz were used**.** 1.0 Hz scan rate and 10 integral gain were first used to image a 10 µm x 10 µm surface area, however, continuous images could not be obtained, as shown in Figure 7. One reason that can explain this situation is that the membrane surface is not quite flat, so a fast scan will cause the tip to get stuck in higher or lower regions. Also, the tip may not respond quickly enough to accurately tracking

the surface. The integral gain was set to 17 because with the higher scan rate, the cantilever

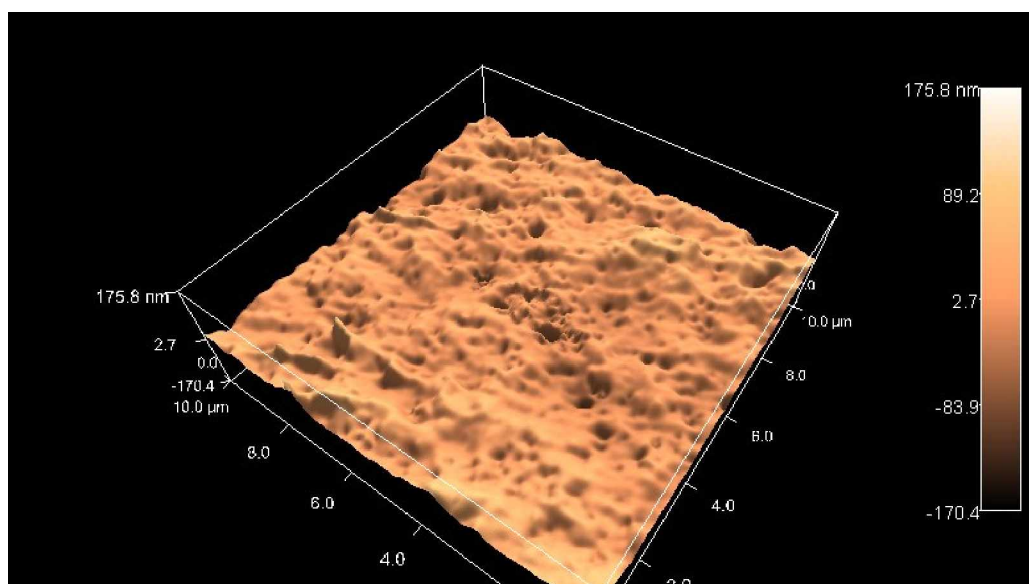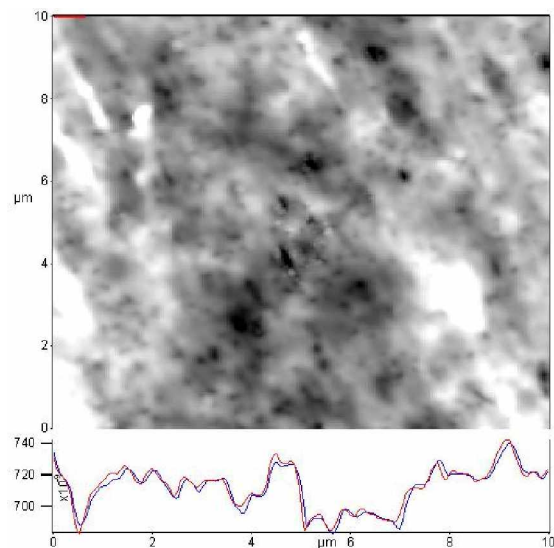should also respond faster to keep the amplitude and phase constant.

Figure 7. Image of a PCTE membrane with 100 nm pores for a scan area of 10 µm x 10 µm. The scan rate is 0.8 Hz. 256 points per line and 256 lines were taken. The set point was set to 800 mV and the integral gain was set to 17. (a) is the height trace
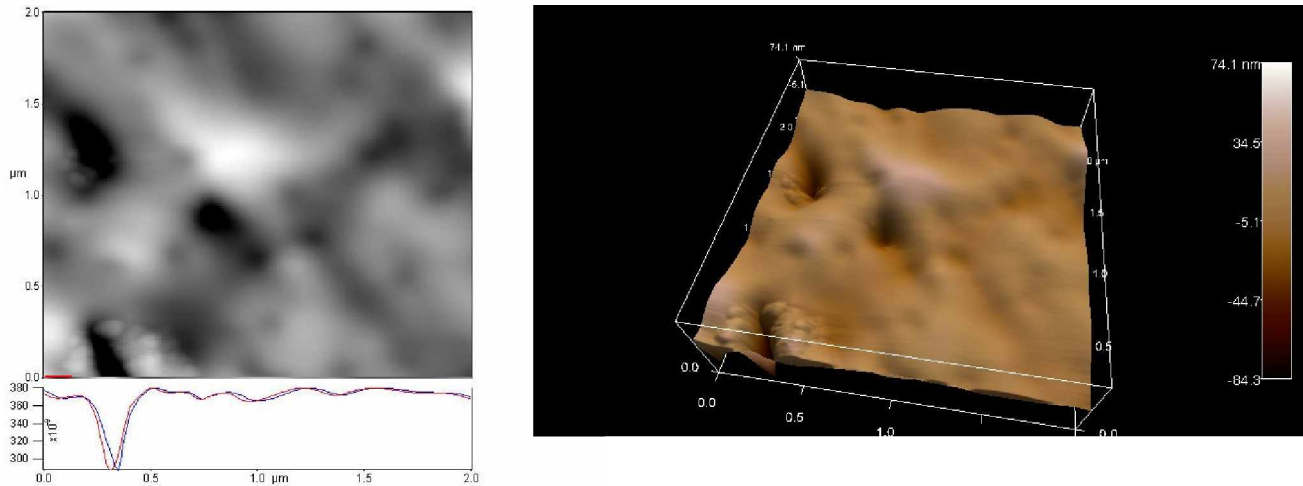(b) is the 3D image.

Figure 8. Image of a PCTE membrane with 100 nm pores for a scan area of 2 µm x 2 µm. The scan rate is 1.0 Hz. 256 points per line and 256 lines were taken. The set point was set to 800 mV and the integral gain was set to 10. (a) is the height trace (b) is the 3D image.

Figure 7 gives us little information about the pores, one possible reason is that the pore is relatively small compared to the scan size. Another possible reason is that the scan rate is too fast for 10 µm x 10 µm scan size since there is not enough time for the tip to go down into the pore to obtain sufficient information.

Figure 8 shows 3 pores in the membrane but the resolution is poor. From the 3D image (Figure 8b), we can see that the depth of the pore is not as expected. One reason could be that the set point is a little too high so that the tip won't go deep into the pore.

2. Sample 2 (tape#3740--membrane--glass slide). A PCTE membrane with 100 nm pores and a silicon 240nm tetra tip with resonant frequency of 70 kHz were used. We were not able to obtain good images of sample 2. The main reason is that the packing tape is too thick (about 72 µm). But the maximum height that the AFM tip can measure is about 60 µm. So the cantilever is actually stuck at the tape, which prevents the tip from touching the membrane surface. But it

appears that the tip was on the surface because of the interaction between the cantilever and the tape.

3. Images of sample 3 (membrane--carbon two-side tape—glass slide). A PCTE membrane with 100 nm pores and a silicon 240 nm tetra tip with resonant frequency of 70 kHz were used.
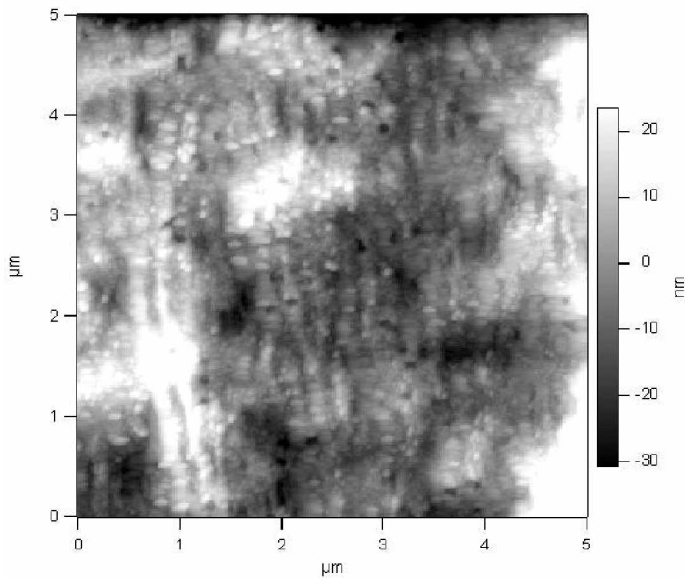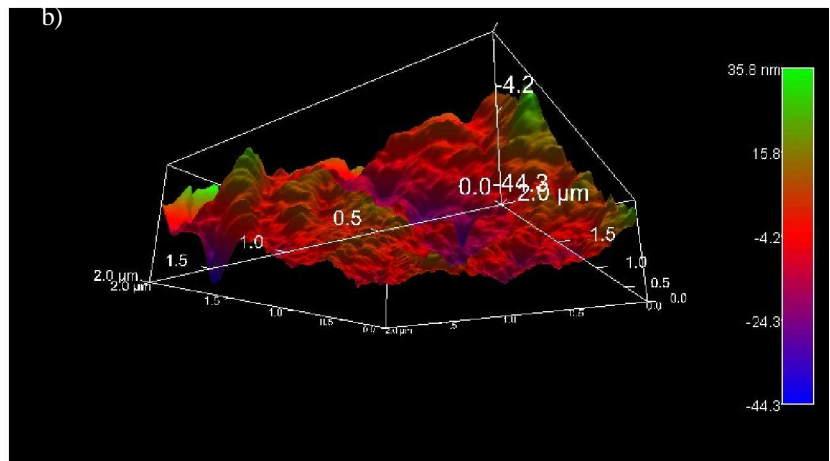

Figure 9. Image (height trace) of a PCTE membrane with 100 nm pores for a scan area of 5 µm x 5 µm. The scan rate is 0.8 Hz. 512 points per line and 512 lines were taken. The set point was first set to 800 mV and the integral gain was set to 17
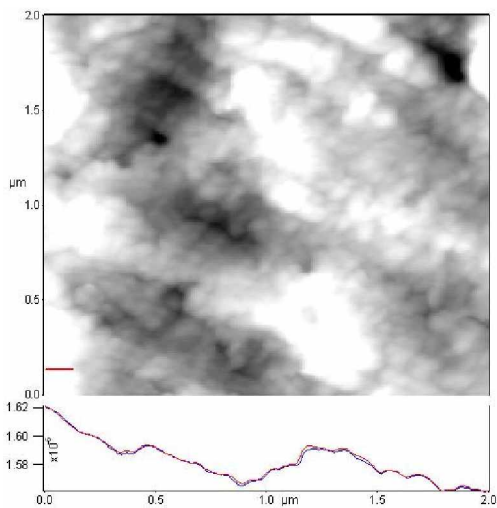

Figure 10. Image of a PCTE membrane with 100 nm pores at scan size of 2 µm x 2 µm. The scan rate is 0.8 Hz. 512 points per line and 512 lines were taken. The set point was first set to 800 mV and the integral gain was set to 17. (a) is the height trace, and (b) is the 3D image.

819

During the scan for Figure 9 the set point was tuned down to 750mV and for figure 10, the set point was tuned down to 700 mV. Higher integral gain was used for both figures. The resolution was enhanced a little but the depth of the pores varies largely from the actual depth. Since lower set point and higher integral gain were used, and the image still could not map the actual surface well, a second type of AFM tip, a silicon 160 nm tetra tip with resonant frequency of 300 kHz was used.
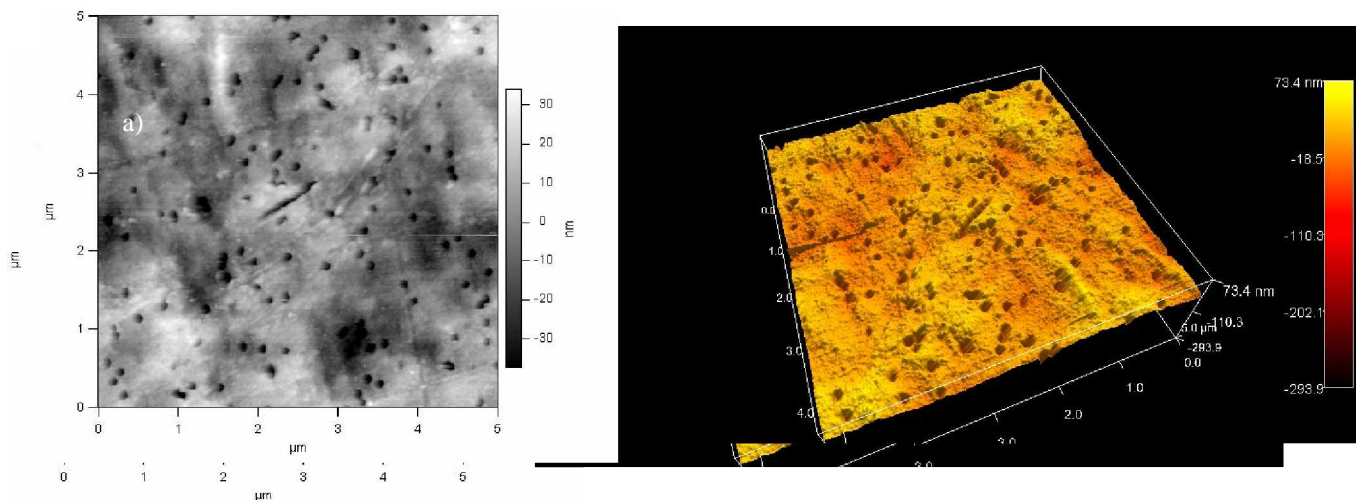

Figure 11. Image of a PCTE membrane with 100 nm pores for a scan area of 5 µm x 5 µm. The scan rate is 0.8 Hz. 512 points per line and 512 lines were taken. The set point was first set to 800 mV and the integral gain was set to 17. (a) is the height trace, and (b) is the 3D image.
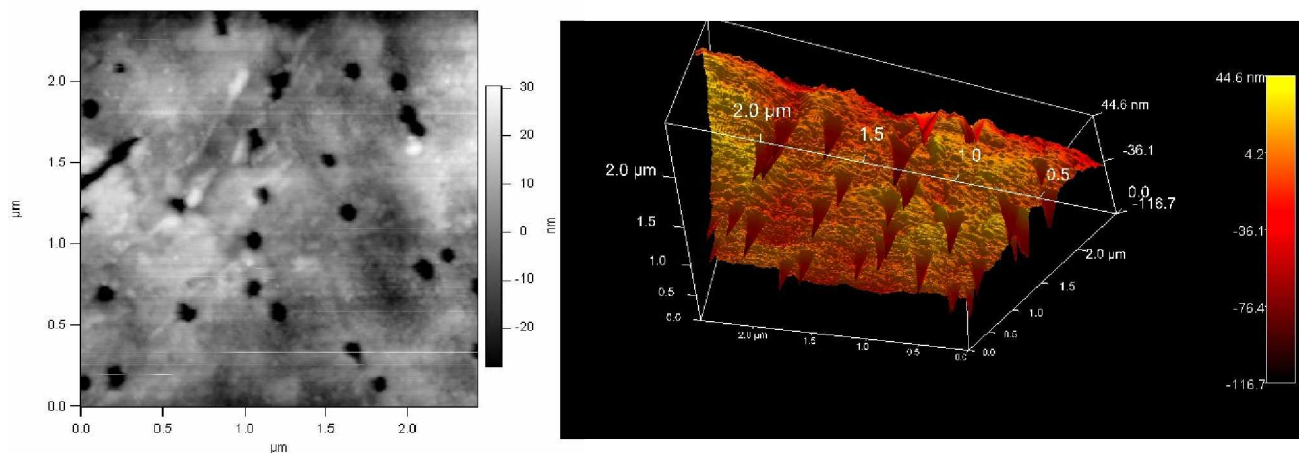

Figure 12. Image of a PCTE membrane with 100 nm pores for a scan area of 2.5 µm x 2.5 µm. The scan rate is 0.8 Hz. 512 points per line and 512 lines were taken. The set point was first set to 800 mV and the integral gain was set to 19. (a) is the height trace, and (b) is the 3D image

Using silicon 160 nm tetra tip with resonant frequency of 300 kHz, high resolution of the surface area was obtained, as shown in Figures 11 and 12. Nanopores can be seen clearly in the images. For 5 µm x 5 µm scan size, the set point was tuned to 780 mV. When the 2.5 µm x 2.5 µm image was taken, a 780 mV set point was not able to keep the tip in contact with the surface. Therefore, the set point was further lowered to 750 mV to make sure the tip was in good contact with the surface.
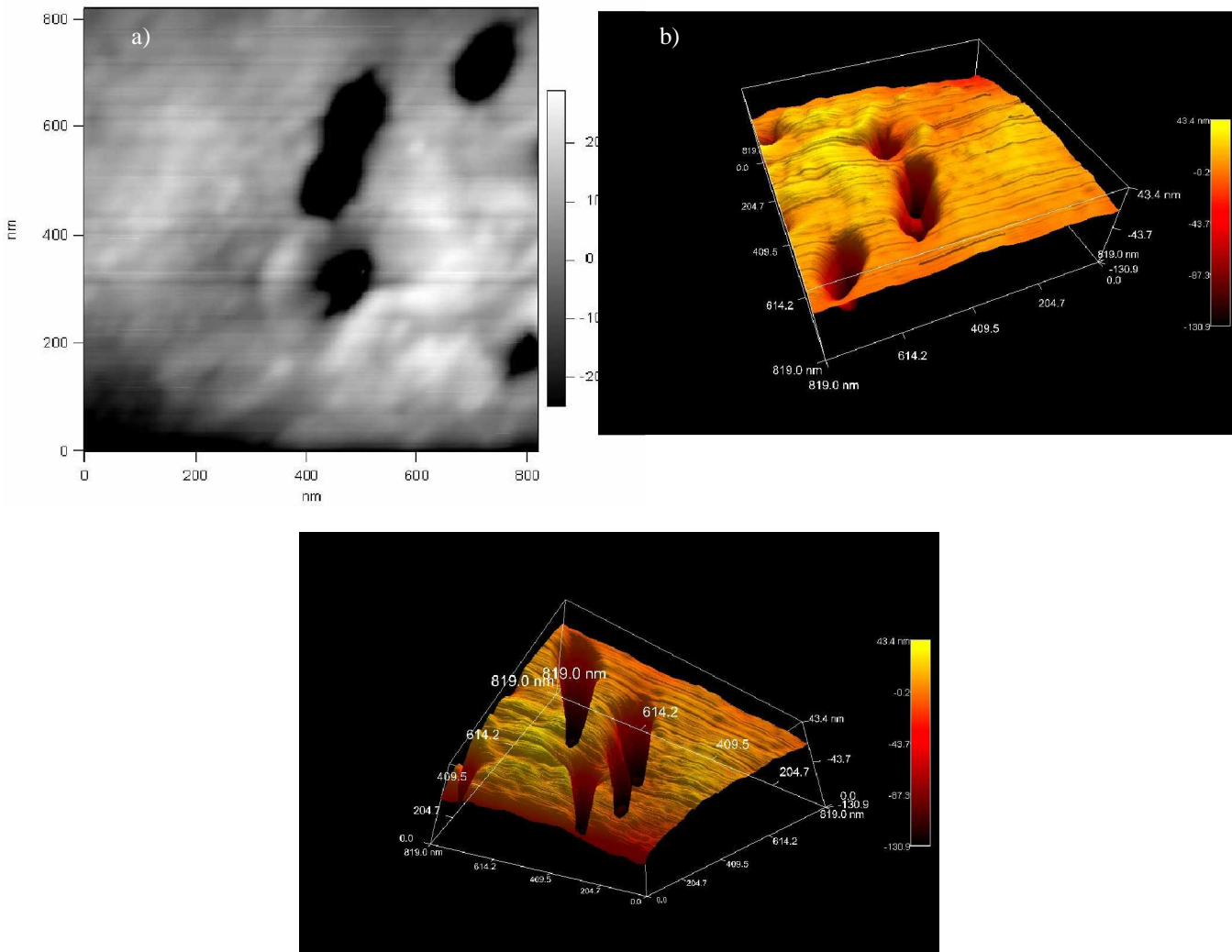

Figure 13. Image of a PCTE membrane with 100 nm pores for a scan area of 0.8 µm x 0.8 µm. The scan rate is 0.6 Hz. 512 points per line and 512 lines were taken. The set point was first set to 800 mV and the integral gain was set to 19. (a) is the height trace, (b) is the 3D image (top view), and (c) is the 3D image (bottom view).

Four nanopores were observed in an 800 nm x 800 nm scan size, as shown in figure 13. The quality of the image is not as good as the 2.5 µm x 2.5 µm and 5 µm x 5 µm images. However, the smaller scan area gives us better information about the individual nanopores. The depth of the nanopore is extremely significant compared to the surface, which is very different from Figures 7, 8, 9 and 10. The set point was tuned even lower to 680 mV, so the tip had better contact with the surface and at the same time, it could penetrate deeper into the nanopore. Also, the scan rate was set to 0.6 Hz so the tip could obtain more information of the surface and the nanopores.

In Figure 14, a PCTE membrane with 50 nm pores and silicon 160 nm tetra tip with resonant frequency of 300 kHz were used. As can be seen, there are some variations in the figure that do not represent the actual surface. This is due to the roughness of surface.
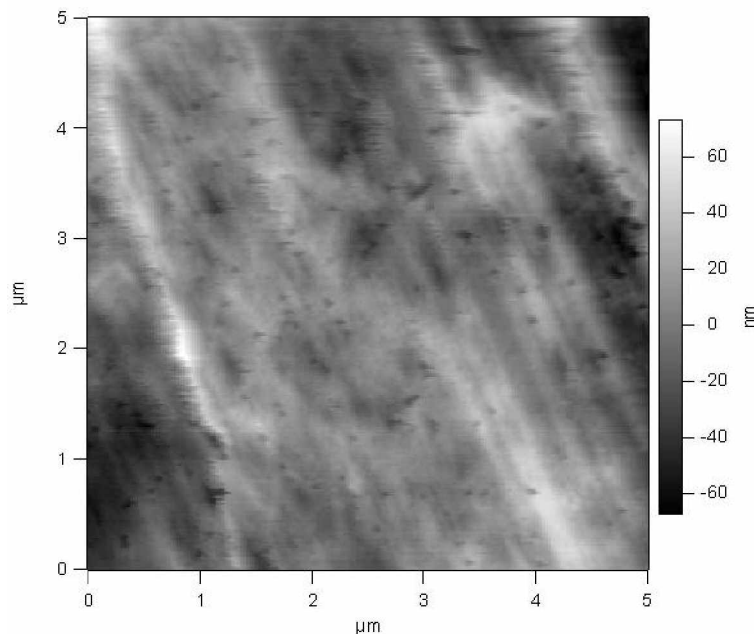

Figure 14. Image (height trace) of a PCTE membrane with 50 nm pores for a scan area of 5 µm x 5 µm. The scan rate is 0.8 Hz. 512 points per line and 512 lines were taken. The set point was first set to 800 mV and the integral gain was set to 10 at first.

AFM is good for flat surface imaging, however if the sample surface is uneven, the tip might not track the surface well. Under this condition, high integral gain should be used and was set to 13.

However, at this point, resonance was observed by the high integral gain, which caused severe loss in resolution. Therefore, feedback was tuned to 11 to eliminate resonance and to optimize the resolution.
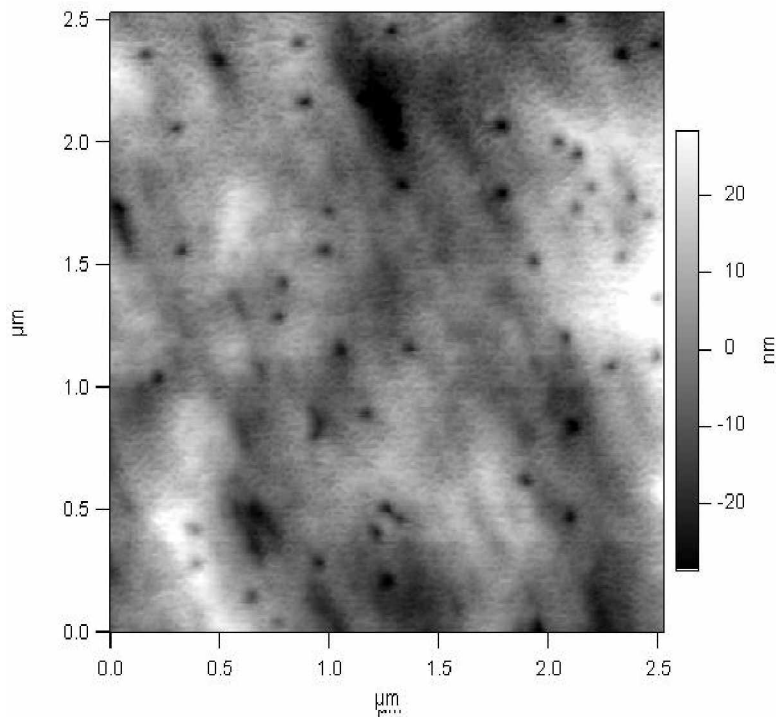

Figure 15. Image (height trace) of a PCTE membrane with 50 nm pores for a scan area of 2.5 µm x 2.5 µm. The scan rate is 0.8 Hz. 512 points per line and 512 lines were taken. The set point was first set to 800 mV and the integral gain was set to 10 at first.

The resolution of Figure 15 is improved, as shown above. The set point was lowered to 700 mV so that when the tip came down from a higher region, it could still press on the lower region. The image area is smaller than the area in Figure 14, which gave more time for the tip to scan across the surface. What is more, the surface is relatively flat in a small region, which also makes it easier for the tip to follow the surface.
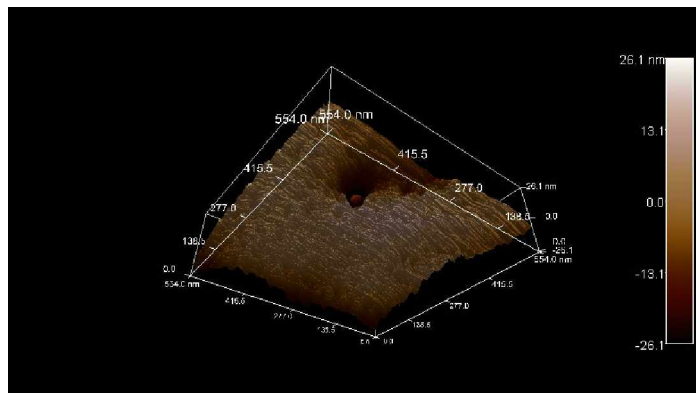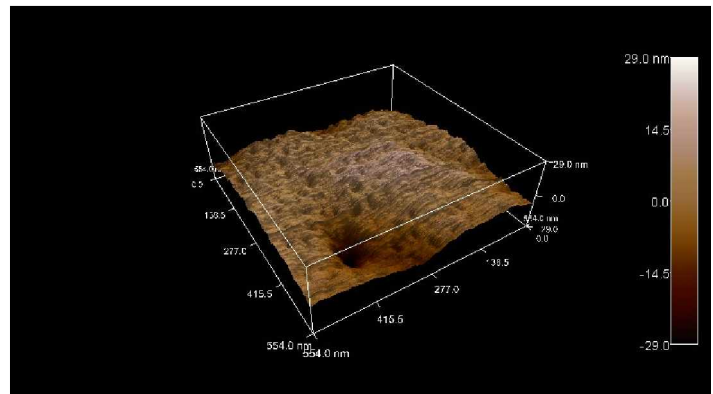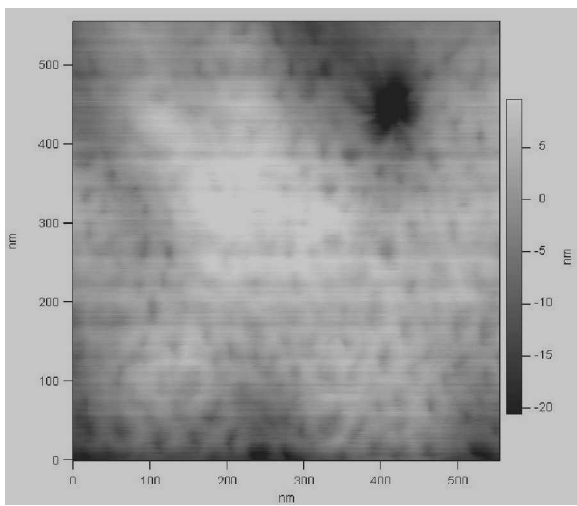
Figure 16. Image (height trace) of a PCTE membrane with 50 nm pores for a scan area of 540 nm x 540 nm. The scan rate is 0.6 Hz. 512 points per line and 512 lines were taken. The set point was first set to 800 mV and the integral gain was set to 19. (a) is the height trace, (b) is the 3D image (top view), and (c) is the 3D image (bottom view)

As shown in figure 16, a single nanopore was successfully imaged by the AFM. The set point was lowered to 670 mV to make the tip in contact with the surface.

A PCTE membrane with 10 nm pores was used and silicon 160 nm tetra tip with resonant frequency of 300 kHz was used. No nanopores were observed because the pore size was 10 nm, which was very close to the tip size (7 nm).

Discussion

PCTE membranes. From the images that we obtained, we can see that nanopores are randomly distributed. For PCTE membrane with 100 nm pores, the pore density is about 3 pores/μm^2. For PCTE membrane with 50 nm pores, the pore density is about 9 pores/μm^2. The pore density from the company for PCTE membrane with 100 nm pores is 4×10^8 pores/m^2, and for PCTE membrane with 50 nm pores is 6×10^8 pores/m^2.

Effects of Sample. One of the major challenges we met in the experiment was the sample preparation. The sample preparation is very important for getting high resolution. The sample should be completely attached to the substrate to avoid vibration when the tip presses on the surface. In the first sample preparation method, it was difficult to ensure that the membrane is completely attached to the substrate, so resolution is poorest among all the images that were taken. In the third sample preparation method, the membrane was better attached to the substrate due to the adhesion of the double-sided carbon tape. As we can see, the images have higher resolution.

Effects of the tip. The tip is one of the crucial factors that affect the resolution of the image. From the experiment, we could see that silicon 160 nm tetra tip with resonant frequency of 300 kHz is better than 240nm tetra tip with resonant frequency of 70 kHz for obtaining images of PCTE membranes with higher resolution. The tips used for imaging is also required to be clean and sharp. Dull or contaminated tip will reduce the resolution.

Effects of other imaging parameters. Scan size, set point, scan rate, and integral gain are other parameters that could be tuned to improve image resolution. From the experiment, we can see that smaller scan area results in a lower set point. If we want to obtain more information about the pore, a lower set point could be used, which means the tip presses harder on the surface. On the other hand, this may cause penetration of the sample and damage to the tip. Slower scan rate means the tip have more time to image at a pixel and average the signal. This will certainly lead to better resolution. However, the scan time is longer. Integral gain is used to control how fast the cantilever will respond to maintain the amplitude at the set point value. It should be set as high as possible. However, if the integral gain is too high, certain resonances will be introduced and will reduce the resolution of the image. So, the integral gain should be to set as high as possible without resonance.

Conclusion

As discussed above, good sample preparation and careful selection of tip are the two most important elements during AFM imaging process. Other parameters should also be well tuned to improve the resolution.

Future work

Future work will focus on liquid phase AFM imaging. Contact mode and tapping mode will be applied to see which one is better for acquiring high resolution. Once we are able to isolate or image a single or several adjacent nanopores we will move on to build nanopore chromatography device. This includes experiments on coating membrane with different materials that have certain selectivity. We will also use electron beam lithography to make holes as small as 100 nm in polymethyl-methacrylate (PMMA). We will use PMMA to cover the membrane and isolate nanopores. Further more, a special sample holder will be designed for conducting AFM experiments. If one dimensional nanopore separation is achieved, we will try multilayer membrane separations, which is expected to significantly enhance fingerprinting of molecules.

References

[1]. Lane A. Baker, Pu Jin, and Charles R. Martin   *Critical Reviews in Solid State and Materials Sciences*, 30, **2005**, 183–205

[2]. S. Yu, S. B. Lee, M. Kang, and C. R. Martin, *Nano Lett.* 1, **2001**, 495.

[3]. J. C. Hulteen, K. Jirage, and C. R. Martin, *J. Am. Chem. Soc.* 120, **1998**, 6603.

[4]. S. B. Lee and C. R. Martin, *Anal. Chem.* 73, **2001**, 768.

[5]. B. B. Lakashmi and C. R. Martin, *Nature* (London, U.K.) 338, **1997**, 758

[6]. S. B. Lee, D. T. Mitchell, L. Trofin, T. K. Nevanen, H. Soederlund, and C. R. Martin, *Science* (Washington, D. C.) 296, **2002**, 2198.

[7]. P. Shao, G. Ji, and P. Chen, *J. Membr. Sci.* 255, **2005**, 1.

[8]. P. Kohli, C. C. Harrell, Z. Cao, R. Gasparac, W. Tan, and C. R. Martin *Science* (Washington, D.C.) 305, **2004**, 984.

[9]. Sergei N. Magonov, Myung-Hwan Whangbo *Surface Analysis with STM and AFM*, **1996**

[10]. Cabral Jean-Louis, Bandilla Dirk, Skinner Cameron D.   *Journal of Chromatography A*, 1108, **2006**, 83–89

the end

[l]

[li] Mastalerz, H.; Menard, M.; Vinet, V.; Desiderio, J.; Fung-Tomc, J.; Kessler, R.; Tsai, Y. *J. Med. Chem.* **1988**, *31*, 1190

[lii] Koerwitz, F. L.; Hammond, G. B.; Wiemer, D. F. *J. Org. Chem.* **1989**, *54*, 738

[liii] Williams, D. R.; Reeves, J. T. *J. Am. Chem. Soc.* **2004**, *126*, 3434

[liv] Williams, D. R.; Reeves, J. T.; Nag, P. P. *Williams Research Group Unpublished Results*

[lv] Williams, D. R.; Reeves, J. T.; Nag, P. P. *Williams Research Group Unpublished Results*

[lvi] Clark, K. B.; Leigh, W. J. *J. Am. Chem. Soc.* **1987**, *109*, 6086

[lvii] Gadwood, R. C.; Lett, R. M. *J. Org. Chem.* **1982**, *47*, 2268-2275

[lviii] Barnier, J. P.; Ollivier, J.; Salaun, J. *Tetrahedron Letters.* **1989**, 2525-2528

[lix] Maurin, P.; Kim, S. H.; Cho, S. Y.; Cha, J. K. *Angew. Chem. Int. Ed.* **2003**, 42, 5044-5047

[lx] ibid

[lxi] ibid

[lxii] Miller, S. A.; Gadwood, R. C. *Org. Syth.,Coll. Vol. VIII* **1991,** 556

[lxiii] ibid

[lxiv] Barnier, J. P.; Ollivier, J.; Salaun, J. *Tetrahedron Letters.* **1989**, 2525-2528

[lxv] ibid

[lxvi] Imamoto, T.; Takiyama, N.; Nakamura, K.; Hatajima, T.; Kamiya, Y. *J. Am. Chem. Soc.* **1989**, *111*, 4392-4398

[lxvii] Maurin, P.; Kim, S. H.; Cho, S. Y.; Cha, J. K. *Angew. Chem. Int. Ed.* **2003**, 42, 5044-5047,
Barnier, J. P.; Ollivier, J.; Salaun, J. *Tetrahedron Letters.* **1989**, 2525-2528

[lxviii] Williams, D. R.; Reeves, J. T.; Nag, P. P. *Williams Research Group Unpublished Results*

[lxix] Buchi, G.; Wuest, H. *Helv. Chem. Acta.* **1979**, 269, 2661-2672

[lxx] Hsu, J. L.; Fang, J. M. *J. Org. Chem.* **2001**, *66*, 8573-8584

[lxxi] Corbel, B.; Medinger, L.; Haelters, J. P.; Sturtz, G. *Synthesis.* **1985**,1048-1051

EXPERIMENTAL SECTION

General Methods:

        All reactions were performed under dry Ar in flame or over dried flasks equipped with Teflon^{TM} stirbars. All flasks were fitted with rubber septa for the introduction of substrates, reagents, and solvents via syringe

        Unless otherwise specified, commercially available reagents were used without further purification. Et_2O and THF were distilled from sodium metal/benzophenone under argon. TMSCl, toluene, $BF_3 \cdot OEt_2$, Et_3N and methacrolein were distilled over CaH_2 under argon. MVK was distilled over K_2CO_3 / $CaCl_2$ under reduced pressure. DMF was taken directly from a 99.99% biological grade bottle.

        ^{1}H NMR spectra were obtained on a Varian VXR-400 (400 MHz) $CDCl_3$ as solvent. ^{13}C NMR were obtained on a Varian VXR-400 (100 MHz) using $CDCl_3$ as solvent. All chemical shifts were recorded in parts per million (ppm) and coupling constants were calculated in hertz (Hz). Mass spectra were obtained on chemical ionization (CIHRMS) or electron impact ionization (EIHRMS) instruments.
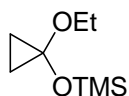
(1-ethoxycyclopropoxy)trimethylsilane (30). See Salaun, J., Marguerite, J. *Org. Synth.,Coll. Vol. VII* **1990**, 131.


1-bromo-1-ethoxycyclopropane (31). See Miller, S. A.; Gadwood, R. C. *Org. Syth.,Coll. Vol. VIII* **1991,** 556.
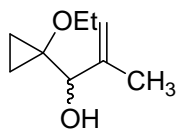
1-(1-ethoxycyclopropyl)-2-methylprop-2-en-1-ol (32). See Miller, S. A.; Gadwood, R. C. *Org. Syth.,Coll. Vol. VIII* **1000,** 556.

t-Butyl lithium (62.1 mL, 1.7 M in pentane) is added dropwise to Et$_2$O (176 mL) at -78 °C and the resulting light yellow mixture is stirred for 30 minutes. Bromide **2** (9.29 g, 56.3 mmol) is added dropwise and the pasty white mixture is stirred for 1 hour. Methacrolein (2.90 mL, 35.2 mmol) is added to Et$_2$O (18 mL) and the solution cooled to -78 °C and added slowly via canulla to the reaction mixture. The cloudy, white mixture is monitored by TLC until the disappearance of starting material, warmed to 0 °C, and quenched with addition of saturated NH$_4$Cl (100 mL). The aqueous layer is extracted with Et$_2$O (3 X 75 mL)and the combined organic extracts are dried over NaSO$_4$, filtered, and concentrated by rotary evaporation to afford a light yellow oil which solidified up cooling. Flash chromatography of the crude (4:1 Hexanes / EtOAc) afforded **3** (5.61 g, 74% yield) as a colourless oil. **^{1}H NMR (400 MHz, CDCl$_3$):** δ 5.03 (s, 1H), 4.88 (s, 1H), 3.98 (s, 1H), 3.56 (dp, 2H), 2.45 (s, 1H), 1.78 (s, 3H), 1.05 (t, 3 H), 0.77 (s, 2H), 0.63 (m, 2H). **^{13}C NMR (100 MHz, CDCl$_3$):** δ 145.3, 111.5, 77.3, 76.7, 19.7, 15.7, 10.4. **IR:** 3445.8, 2975.14, 2876.68, 1652.21, 1453.28. **R$_f$:** 0.41 (4:1 Hexanes / EtOAc).
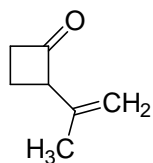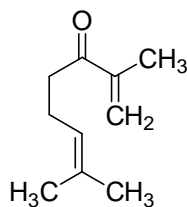

2-(prop-1-en-2-yl)cyclobutanone (33). See Barnier, J. P.; Ollivier, J.; Salaun, J. *Tetrahedron Letters.* **1989**, 2525-2528.
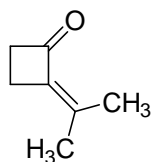
A solution of **3** (9.83 g, 62.9 mmol) in Et$_2$O (315 mL) stirred with cooling at -78 °C. BF$_3$·OEt$_2$ (7.90 mL, 62.9 mL) is added dropwise to the solution and the reaction is allowed to warm to room temperature and monitored by the consumption of starting material by TLC. The reaction is carefully quenched with saturated NH$_4$Cl (200 mL) and extracted with ether. The combined organic extracts are dried over MgSO$_4$, filtered, and concentrated by rotary evaporation to afford a dark yellow oil. Flash chromatography of the resulting crude (9:1 Hexanes / EtOAc) afforded **4** (6.93 g, 87% yield) as a light yellow oil. **^{1}H NMR (400 MHz, CDCl$_3$):** δ 4.83 (d, *J* = 8.8 Hz, 2H), 3.91
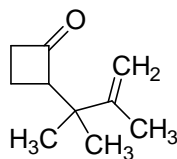
(t, 1H), 3.05 (m, 1H), 2.92 (m, 1H), 2.20 (m, 1H), 2.03 (m, 1H), 1.78 (s, 3H). **^{13}C NMR (100 MHz, CDCl$_3$):** δ

208.2, 140.0, 110.8, 66.7, 44.4, 21.2, 15.3. **IR:** 2971.4, 2359.5, 2349.4, 1785.15, 1646.3. **R$_f$:** 0.7 (4:1

Hexanes/EtOAc). **HRCIMS:** [M]$^+$ obsd 110.0722, calc for C$_7$H$_{10}$O 110.0732.

2,7-dimethylocta-1,6-dien-3-one (35). See See Barnier, J. P.; Ollivier, J.; Salaun, J. *Tetrahedron Letters.* **1989**,

2525-2528.

2-(propan-2-ylidene)cyclobutanone (34).

2-(2,3-dimethylbut-3-en-2-yl)cyclobutanone (36).

A solution of **4** (0.500 g, 4.54 mmol) in THF (32 mL) is stirred with cooling at -78 °C. 2-propenylmagnesium

bromide (13.6 mL, 0.5 M in THF) is added dropwise to the solution via syringe, and the reaction is allowed to

warm to room temperature. The reaction is monitored by the consumption of starting material by TLC and

quenched with saturated NH$_4$Cl (50 mL). The aqueous layer is extracted with Et$_2$O (3 X 25 mL) and the combined

organic fractions are dried over Na$_2$SO$_4$, filtered, and concentrated by rotary evaporation to give a dark yellow oil. The resulting crude is purified by flash chromatography (95:5 Hexanes / EtOAc) to give **5**, **6**, and **7** respectively.

(5) : ^{1}H NMR (400 MHz, CDCl$_3$): δ 5.93 (s, 1H), 5.73 (s, 1H), 5.08 (t, 1H), 2.69 (t, 2H), 2.27 (m, 2H), 1.85 (s, 3H), 1.66 (s, 3H), 1.60 (s, 3H). ^{13}**C NMR (100 MHz, CDCl$_3$):** δ 201.7, 144.4, 132.4, 123.0, 122.8, 37.5, 25.5, 23.1, 17.6, 17.5. **R$_f$:** 0.74 (4:1 Hexanes / EtOAc).

(6) : ^{1}H NMR (400 MHz, CDCl$_3$): δ 2.80 (t, 2H), 2.49 (m, 2H), 2.06 (m, 3H), 1.74 (s, 3H). **R$_f$:** 0.56 (4:1 Hexanes / EtOAc).

(7) : ^{1}H NMR (400 MHz, CDCl$_3$): δ 5.03 (m, 1H), 4.82 (m, 1H), 2.49 (m, 1H), 2.21 (m, 2H), 1.99 (m, 2H), 1.82 (s, 3H), 1.65 (s, 3H), 1.57 (s, 3H). **R$_f$:** 0.48 (4:1 Hexanes / EtOAc). **HRCIMS:** [M-H]$^+$ obsd 151.1120, calc for C$_{10}$H$_{15}$O 151.1117.
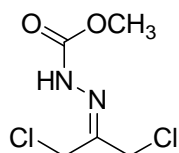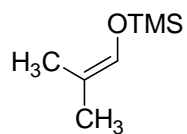

methyl 2-(1,3-dichloropropan-2-ylidene)hydrazinecarboxylate (53). See Corbel, B.; Medinger, L.; Haelters, J. P.; Sturtz, G. *Synthesis.* **1985**,1048-1051.
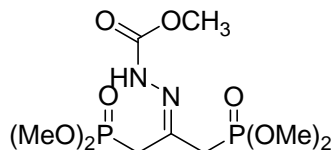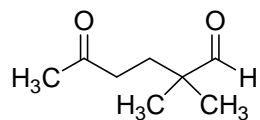

Bisphosphonate hydrazone (54). See Corbel, B.; Medinger, L.; Haelters, J. P.; Sturtz, G. *Synthesis.* **1985**,1048-1051.
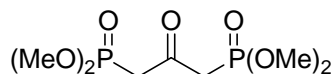
tetramethyl 2-oxopropane-1,3-diyldiphosphonate (42). **See Corbel, B.; Medinger, L.; Haelters, J. P.; Sturtz, G. *Synthesis.* 1985,1048-1051.**

trimethyl(2-methylprop-1-enyloxy)silane (51). See Hsu, J. L.; Fang, J. M. *J. Org. Chem.* **2001**, *66*, 8573-8584.

2,2-dimethyl-5-oxohexanal (41). See Hsu, J. L.; Fang, J. M. *J. Org. Chem.* **2001**, *66*, 8573-8584.